JGR Solid Earth

RESEARCH ARTICLE
10.1029/2019JB017541

Deriving Rupture Scenarios from Interseismic Locking Distributions Along the Subduction Megathrust

Hongfeng Yang[1], Suli Yao[1], Bing He[1,2], Andrew V. Newman[3], and Huihui Weng[1,4]

[1]Earth System Science Programme, The Chinese University of Hong Kong, Hong Kong, [2]Now at Graduate School of Oceanography, The University of Rhode Island, Kingston, RI, USA, [3]School of Earth and Atmospheric Sciences, Georgia Institute of Technology, Atlanta, GA, USA, [4]Now at Universite Cote d'Azur, IRD, CNRS, Observatoire de la Cote d'Azur, Valbonne, France

Abstract Given recent advances in geodetic data, interseismic locking models along the megathrust now become useful to qualitatively evaluate future earthquake potential. However, an individual earthquake's true rupture potential is challenging, as it depends on more than just a static image of prior locking. Here, we test the determinism of interseismic locking models using spontaneous rupture simulations and the well-resolved processes associated with the 2012 moment magnitude (Mw) 7.6 Nicoya earthquake. To do so, we estimate initial megathrust stress from locking by assuming that the entire slip deficit will be released in the next megathrust earthquake. Then we initiate spontaneous ruptures at the hypocenter of the 2012 Nicoya earthquake. We find scenarios that approximate the same coseismic slip distribution and final earthquake moment magnitude as obtained from seismic and geodetic observations, demonstrating that deriving potential rupture scenarios from interseismic locking is feasible. We also find that spontaneous rupture scenarios from different locking models differ in moment rate duration and thus ground motion prediction, although the final slip distribution and moment magnitude were similar. The results highlight that quantifying rupture scenarios and ground motions from reliable locking models by dynamic rupture simulations can be an effective tool for seismic hazard assessment in subduction zones.

Key Points:
- We conduct numerical simulations of rupture scenarios based on interseismic locking models
- Our simulated earthquake scenario is well consistent with kinematic models of the 2012 Mw 7.6 Nicoya earthquake
- Details of rupture process and synthetic waveforms depend on the choice of the input locking model

Supporting Information:
- Supporting Information S1
- Movie S1

Correspondence to:
H. Yang,
hyang@cuhk.edu.hk

Citation:
Yang, H., Yao, S., He, B., Newman, A. V., & Weng, H. (2019). Deriving rupture scenarios from interseismic locking distributions along the subduction megathrust. *Journal of Geophysical Research: Solid Earth*, *124*. https://doi.org/10.1029/2019JB017541

Received 16 FEB 2019
Accepted 9 SEP 2019
Accepted article online 12 SEP 2019

1. Introduction

The interseismic locking distribution derived from geodetic measurements has significantly improved our understanding of a future earthquake's potential along a variety of subduction zones (e.g., Konca et al., 2008; Loveless & Meade, 2011; Satake & Atwater, 2007). The locked patches are often interpreted as where megathrust earthquakes will occur, which has been shown true in at least a few cases, including the Maule and Iquique region of Chile (Metois et al., 2013; Moreno et al., 2010), the central Peru megathrust (Perfettini et al., 2010), and northern Costa Rica (Protti et al., 2014). However, it is difficult to directly infer future rupture extent based on the locking distribution, as shown in the southern Chile subduction zone where the 2010 Mw 8.8 Maule and 2015 Mw 8.3 Illapel earthquakes ruptured a portion of the highly locked patch (Moreno et al., 2010; Yin et al., 2016), respectively, leaving a ~50-km-long locked segment unbroken in between. Similarly, partial rupture of a locked patch has also been found on the Sumatra megathrust during the 2007 Mw 7.9 and Mw 8.4 earthquakes (Konca et al., 2008). Thus, it remains challenging for seismic hazard evaluation to accurately estimate future rupture extents from locking models.

Even though the interseismic locking distribution can be used to map out the potential ruptures in certain regions, details of the rupture process cannot be inferred from those static locking images. For instance, in the case of static locking models, patches of higher locking are sometimes expected to slip more in future earthquakes. In the case of the 2007 Mw 8.0 Pisco earthquake, two major rupture patches were observed, with the larger one coinciding with a zone of intermediate locking (Perfettini et al., 2010). Furthermore, numerical simulations based on interseismic locking models in the Nicoya Peninsula of Costa Rica show that different nucleation locations may lead to completely different rupture scenarios (Yang et al., 2019). Due to the rupture directivity effect, the ground displacement in the offshore region of a downdip nucleating rupture is nearly twice as much as that from an updip nucleating rupture, despite the identical initial loading conditions and ultimate moment magnitudes of the two scenarios (Yang et al., 2019). Such enlarged ground displacement on the seafloor may increase the tsunamigenic potential. The dependence of rupture scenarios on hypocenter locations also highlights the advantage of deriving rupture details from dynamic rupture simulations, which can better prepare for earthquake and tsunami hazard assessment in subduction zones.

Efforts have been made to quantitatively evaluate interseismic locking models for dynamically driven coseismic slip (e.g., Hok et al., 2011; Lozos et al., 2015; Yang et al., 2012). For example, in a rate- and state-dependent friction model to evaluate long-term rupture characteristics, Kaneko et al. (2010) have found an unlocking (velocity strengthening) region could be broken by accumulated stress due to ruptures on the neighboring locked (velocity weakening) segments. The probability for an earthquake to break through the velocity-strengthening patch correlates with the average degree of interseismic locking. In contrast with such generic models of earthquake cycles, coseismic rupture scenarios for specific subduction zones have been built on interseismic locking models, such as in Nankai Trough, Japan, where rupture extent was governed by the prescribed along-strike variation in fracture energy (Hok et al., 2011). In Cascadia, Yang, Liu, and McGuire (2012) have derived potential rupture scenarios using two locking models to estimate initial stress distribution (Burgette et al., 2009; McCaffrey et al., 2007) and suggest that rupture extents are dependent on hypocenter locations. Due to the long recurrence intervals between large earthquakes in Nankai, Cascadia, and many other subduction zones, the above numerical simulation results have not yet been able to compare with field observations recorded by modern instruments. Consequently, it is intrinsically difficult to judge whether the model assumptions and critical parameters in these studies are reasonable for real subduction environments. Validating such quantitative rupture scenarios with observed coseismic slip is necessary.

To derive rupture scenarios from interseismic locking and validate such scenarios with observed coseismic slip, a megathrust rupture that is well resolved from modern instrumental records, such as the one below the Nicoya Peninsula, is desired to compare with the numerical coseismic process. As such, we conduct spontaneous rupture simulations based on the interseismic locking distribution here, where the Cocos plate consisting of the East Pacific Rise and the Cocos-Nazca crust subducts beneath the Caribbean plate at a rate of ~82 mm/year (DeMets et al., 2010; Harris et al., 2010; Figure 1). On 5 September 2012, an Mw 7.6 earthquake occurred directly under the peninsula, consistent with one of the previously determined locked patches (Protti et al., 2014; Yue et al., 2013). The instrumentally well recorded 2012 Nicoya earthquake provides us an unprecedented opportunity to quantitatively evaluate coseismic slip from interseismic locking distribution using numerical simulations.

In this paper, we first introduce kinematic source models of the 2012 Nicoya earthquake and the locking models that are used to constrain slip deficit. Then we describe the model setup and how to convert the locking distributions into initial stress condition. We also conduct a series of sensitivity tests in deriving the rupture scenarios, including material properties and rupture nucleation from the hypocenter of the 2012 Nicoya earthquake. In comparison, rupture scenarios in the recent work of Yang et al. (2019) were nucleated from a number of prescribed locations in the locked region. Next we validate our preferred rupture scenarios with kinematic source models and ground velocities of the Nicoya earthquake, which was not available in Yang et al. (2019). We also discuss potential factors that could affect rupture propagation. In the end we conclude that deriving a reasonable rupture scenario from interseismic locking distribution is feasible and can be used in evaluating seismic hazards in subduction zones.

2. Interseismic Locking Models in the Nicoya Peninsula and the 2012 Nicoya Earthquake

The rapid convergence between the Cocos and the Caribbean plates (~82 mm/year) in the Middle America subduction zone produced a series of large M~7.5+ earthquakes in the Nicoya Peninsula with an approximate 50-year recurrence interval, the prior event being in 1950 (Protti et al., 2001). The Nicoya Peninsula of northwestern Costa Rica lies only ~40 km from the trench (Figure 1), forming a unique environment allowing near-field on-land geodetic observations directly above the seismogenic portion of the megathrust. A late interseismic locking distribution derived from trench-normal and vertical campaign and continuous global positioning system (GPS) data revealed two fully locked patches that were capable of generating up to an Mw 7.8 earthquake (Feng et al., 2012). Using the identical megathrust fault geometry, Xue et al. (2015) updated the locking model by adding trench-parallel GPS and line-of-site interferometric synthetic aperture radar data. Despite the variations in locking maps in both downdip and along-strike directions, two locked patches were imaged near the coastline of central Nicoya, roughly 60 km in length along strike in both locking models (Figure 1). A large earthquake was anticipated over the locked patches given the large earthquake history and the strain accumulation that was imaged on the interface.

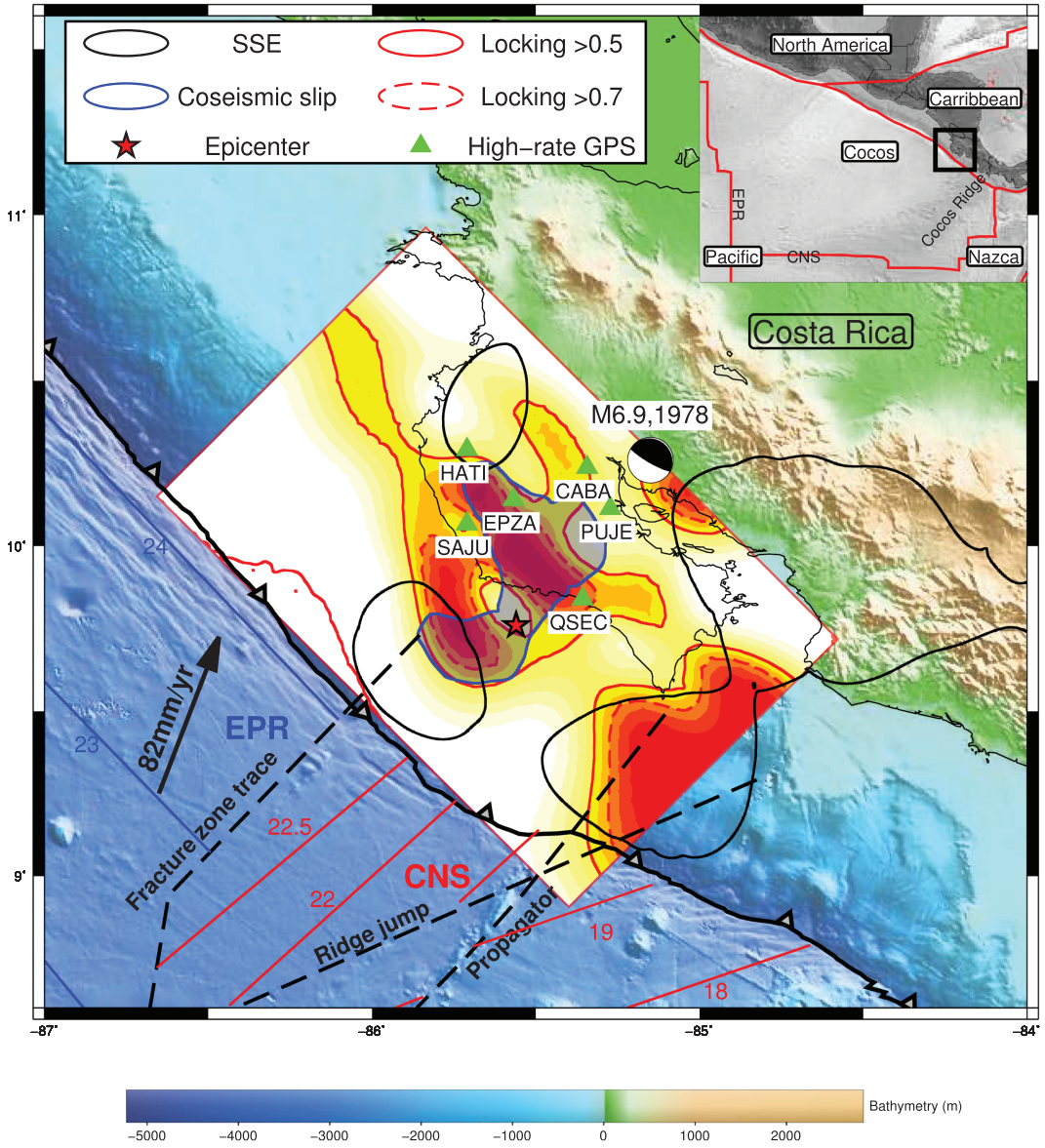

Figure 1. Tectonic setting of the Nicoya Peninsula. Xue's interseismic locking (2015) and coseismic slip (Yue et al., 2013) of the 2012 Nicoya earthquake (>1 m) are shown in red and blue filled polygons. Red star denotes the earthquake epicenter. Green triangles denote high-rate global positioning system (GPS) stations that recorded the 2012 earthquake. Areas with slow slip events (Dixon et al., 2014) are shown in black polygons. Solid blue and red lines denote plate age in the incoming plate while dashed lines show tectonic boundaries (Barckhausen et al., 2001). EPR = East Pacific Rise; CNS = Cocos-Nazca spreading center.

On 5 September 2012, an Mw 7.6 earthquake (hereafter called the Nicoya earthquake) occurred directly over the previously determined locked patches with the rupture nucleating offshore (Yue et al., 2013), resulting in a coseismic uplift up to ~0.7 m (Protti et al., 2014). The coseismic slip distributions determined from static GPS observations showed that the Nicoya earthquake ruptured the landward extent of the locked patch, with a maximum slip of ~4 m (Protti et al., 2014). Joint inversion results using multiple sources of data such as teleseismic *P* waves and local strong motion and GPS observations indicated that the rupture propagated at a velocity of ~3.0 km/s and broke two patches with an average slip of ~2 m in the primary slip zone (Liu et al., 2015; Yue et al., 2013). Moment rate functions showed a relatively simple rupture process, with a single peak value of $2.3 - 2.7 \times 10^{19}$ Nm/s (Quintero et al., 2014; Ye et al., 2013).

3. Method and Model Parameter

Key ingredients to simulating dynamic ruptures include fault geometry and material properties, as well as appropriately estimating the initial stress distribution and fault friction (e.g., Harris, 2004). In this section we describe how we set up the finite element model, estimate the initial stress and strength distribution, and conduct resolution tests for spontaneous rupture scenarios. All computations are conducted using a finite element package, Pylith (Aagaard et al., 2013), which was well tested in spontaneous rupture simulation exercises (Harris et al., 2018).

3.1. Megathrust Geometry and Frictional Law

In order to make meaningful comparison of our numerical results and linking the interseismic deformation to coseismic rupture process, we incorporate a smoothly curved fault geometry that was used to invert for the locking models (Feng et al., 2012, hereafter Feng locking model; Xue et al., 2015, hereafter Xue locking model) and the coseismic rupture process (Yue et al., 2013). We construct a three-dimensional mesh in an elastic domain, which extends 180 km along strike, 170 km perpendicular to strike, and 80 km at depth. The geographical reference point is at (−85.40, 8.91) and rotated N45°W, the approximate strike of the trench (Figure 1). Following the fault geometry used in the locking models, the fault interface starts at 4.5 km in depth below the sea level.

We assume that the fault is governed by Ida's (1972) linear slip-weakening law, which is widely used in spontaneous rupture simulations (e.g., Ampuero et al., 2002; Andrews, 1976, 1985; Day, 1982; Olsen et al., 1997; Palmer & Rice, 1973; Weng et al., 2015). Parameters in the linear slip-weakening law include yield strength, initial and dynamic stresses, and the critical slip distance d_0. According to the seismological source observations, the d_0 is suggested to be proportional to final slip (Tinti et al., 2005). However, it is well known that determination of d_0 after an earthquake suffers from a trade-off with yield strength (Guatteri & Spudich, 2000). Recent investigations integrating spontaneous rupture simulation and near-field observations yield robust estimates of in situ d_0 during the 2015 Mw 7.8 Nepal and 2012 Mw 7.6 Nicoya earthquakes, which are one fifth the final slip magnitude (Weng & Yang, 2018; Yao & Yang, 2018). Their results also show that given nonuniform prestress distribution, the rupture process and synthetic ground velocities generated from a heterogeneous distribution of d_0 do not significantly differ with those using a uniform average value of d_0 (Weng & Yang, 2018). As we do not know the amplitude of future coseismic slip, we set a uniform d_0 of 0.4 m on the fault plane, a value commonly used in spontaneous rupture simulations (e.g., Harris et al., 2009).

3.2. Distribution of Initial Stress, Dynamic Stress, and Yield Strength

We estimate the stress state on the fault from slip deficit pattern, which in turn is inferred from interseismic locking distribution. To do so, we make the following assumptions. First, the slip deficit is linearly and continuously accumulated during the period of stress buildup, following Hok et al. (2011). Although the locked depth has been suggested nonstationary with updip propagating creep in other subduction zones (e.g., Bruhat & Segall, 2017), the well-documented characteristic earthquakes below Nicoya indicates that the locked patches probably do not significantly change spatially (Protti et al., 2001). Temporal changes of locking degrees are possible, as partial ruptures of the locked patches may occur in small to moderate earthquakes. However, interplate earthquakes in the Nicoya region with magnitudes larger than 6 were rare before the 2012 event, except the 1978 Mw 6.9 earthquake whose centroid location in the Global Centroid Moment Tensor catalog is further inland (Figure 1). Although relocation indicates this event occurred at a much shallower depth, probably on the megathrust near coast (Avants et al., 2001), the location uncertainty is relatively large. Furthermore, moment released during an Mw 6.9 and smaller quakes can only slightly affect our estimated slip deficit. Moreover, the observed slow slip events in the Nicoya region surrounded but had little overlap with the locked region (Dixon et al., 2014) and thus would not release the accumulated stress (Figure 1). Instead, the locked patches may be loaded by slow slip events. Therefore, the first assumption appears to be valid in the Nicoya Peninsula. Although the aforementioned processes may lead to uncertainties of our estimated slip deficit, it would not significantly change the moment magnitude and final slip distribution of rupture scenarios, by considering up to 15% perturbation in the estimated slip deficit (Yang et al., 2019). As such, we obtain the slip deficit from the long-term slip rate (~82 mm/year) and the interseismic locking distributions.

Second, we assume that the accumulated stress will be completely released by a large earthquake. Since the last Mw 7.5+ earthquake below the Nicoya Peninsula was in 1950, we then obtain the stress buildup $\Delta\tau$ from the slip deficit for 62 years (1950–2012), which is assumed to be the static stress drop for a future earthquake. The slip deficit is assumed purely along the dip direction, as indicated by the locking models. To compute the stress buildup from the slip deficit, we set all boundaries in the domain as Dirichlet boundary conditions (i.e., displacement is fixed) except the free surface. Since the domain is sufficiently large, the results are presumably not affected by the boundary conditions (e.g., Yin et al., 2016, 2017). Furthermore, we compare our numerical results of stress changes with half-space analytical solutions that are calculated from a triangular element dislocation method (Meade, 2007). We compute the stress changes for 1-year slip deficit from the Feng locking model. The numerical results and analytical results show remarkable coherence (Supporting Information, Figure S1), reassuring that our computation of stress changes is not affected by the boundaries.

To estimate the initial stress τ_0 before the 2012 earthquake, we assume a constant dynamic friction coefficient (i.e., 0.2) that is indicated from fast sliding laboratory experiments (Di Toro et al., 2011). For simplicity, the effective normal stress is taken as 50 MPa, assuming near-lithostatic pore pressure on the megathrust (Saffer & Tobin, 2011). Therefore, the heterogeneous initial stress field is the sum of the dynamic stress (10 MPa) and static stress drop (Figure 2). The yield stress is assumed to be slightly higher than the maximum initial stress (Hok et al., 2011), and thus we set the static coefficient as 0.41 (Table 1). We also test scenarios with spatially varying strengths (rupture scenario 2 in Table 1) that will be discussed later. A higher static friction coefficient (e.g., 0.6) can produce similar results with a smaller critical slip-weakening distance, which demands more computational power. As such, we use the values in Table 1 for our simulations.

3.3. Effects of Material Properties

The initial stress computation is dependent on the material properties. We compare the values of stress level for a half-space model and a one-dimensional depth-dependent velocity structure (Table S1), which was inferred from the results of seismic receiver function and tomographic images in the region (Audet & Schwartz, 2013; DeShon et al., 2006) and was also used in the kinematic source model for the 2012 Nicoya earthquake (Yue et al., 2013). Amplitudes in the calculated stress levels at greater depth in the one-dimensional velocity model are larger than the half-space model, due to the increasing shear modulus (Figures 3a and 3b). In the highly locked region where the 2012 earthquake occurred, the difference is smaller than 1 MPa.

However, the dynamic rupture scenarios with different materials do not exhibit distinct differences, including final slip distribution and moment magnitudes (Figures 3c and 3d). We apply those two heterogeneous initial stress fields and their respective material models in spontaneous rupture simulations. Ruptures are nucleated from the hypocenter of 2012 Mw 7.6 earthquake. Although there are minor differences in slip amplitudes at different portions, the overall slip distribution and final moment magnitudes are not significantly dependent on the material properties (Figure 3). Thus we use a half-space in our dynamic rupture models.

3.4. Resolution Tests of Coseismic Rupture Process

In order to satisfy numerical requirements to resolve the rupture front, the cohesive zone where the stress decreases from the static to dynamic state must be 3 to 5 times larger than the grid size (Day et al., 2005). The size of the static cohesive zone equals to

$$\Lambda_0 = \frac{9\pi}{32}\frac{\mu}{1-\nu}\frac{d_0}{\tau_s-\tau_d}, \tag{1}$$

where μ is shear modulus, ν is Poisson's ratio, d_0 is critical slip distance, and τ_s and τ_d are the static and dynamic shear stress, respectively. According to the parameters used in our models (Table 1), the static cohesive zone size equals to 1.46 km, so the mesh grid size x_0 should be smaller than 500 m.

Note that the dynamic cohesive zone size is smaller than the static one (Day et al., 2005). Therefore, we tested mesh grid sizes of 400, 300, 250, and 200 m on the fault interface during dynamic rupture simulations. The results show that the final slip patterns are stable for 300, 250, and 200 m, while the slip amplitudes and moment magnitudes slightly differ (Figure S2). Based on the grid size test, we select 250 m as the

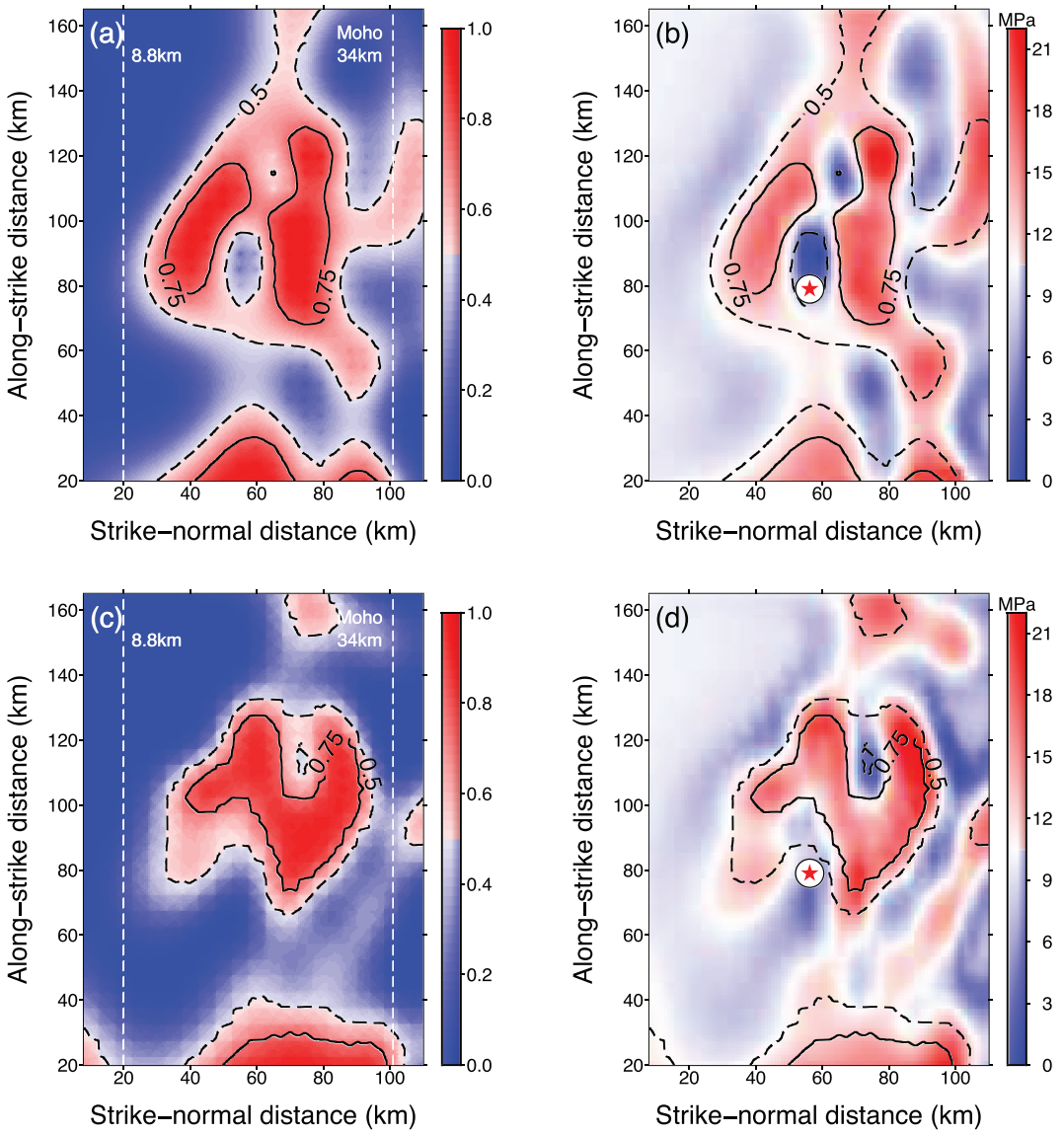

Figure 2. Interseismic locking distribution—(a) Xue's locking model (c) Feng's locking model—and the initial stress estimations from the two locking models, respectively. Star denotes epicenter of the 2012 Nicoya earthquake (Yue et al., 2013).

preferred grid size for the fault and gradually increase the grid to 3 km at the remote boundaries to reduce computation time. All boundaries aside from the free surface are set to be absorbing boundary conditions to avoid the interference from the boundary-reflected waves.

Table 1
Model Parameters in Dynamic Rupture Simulations

Fault parameter	Rupture scenario 1	Rupture scenario 2
Static friction coefficient, f_s (strength/σ_n)	0.41	Northwest: 0.45 Southeast: 0.37
Dynamic friction coefficient, f_d	0.2	0.2
Effective normal stress, σ_n (MPa)	50	50
Critical slip distance, d_0 (m)	0.4	0.4

The time step Δt is set as 0.007 s based on the minimum tetrahedron element size, and thus the Courant-Friedrichs-Lewy ratio, $CFL = V_p \Delta t / \Delta x = 0.2 < 0.71$, satisfies the CFL condition and numerical requirements for dynamic rupture process (Madariaga, 1976).

4. Deriving Rupture Scenarios from Interseismic Locking Models

4.1. Nucleation with Heterogeneous Initial Stress

How natural earthquakes nucleate remains controversial based on observations to date (Ellsworth & Bulut, 2018; Tape et al., 2018). In

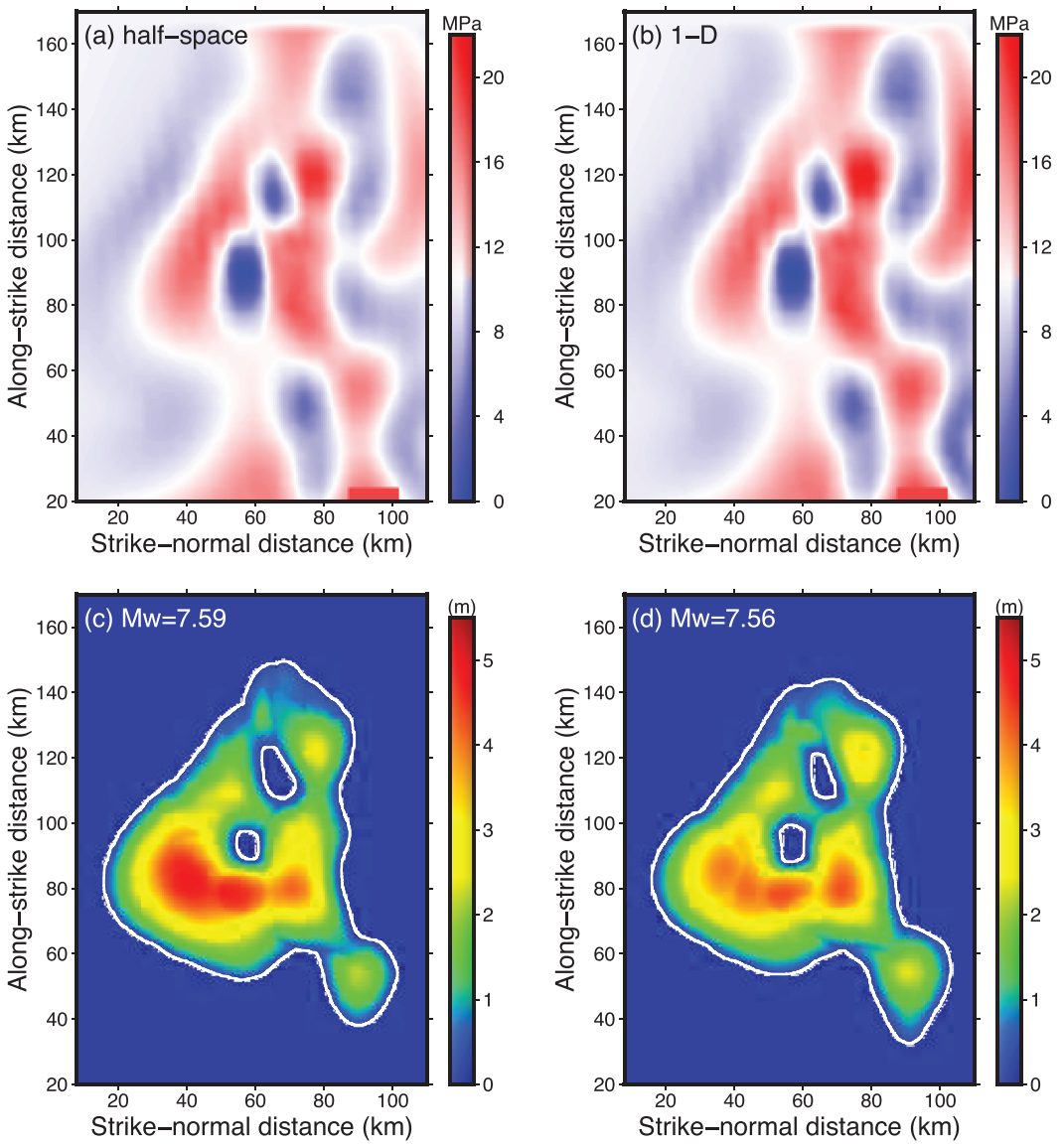

Figure 3. Initial stress (a and b) and rupture scenarios (c and d) for two types of material properties obtained from the Xue locking model. (a and c) A homogeneous half-space model. (b and d) A one-dimensional depth-dependent velocity model.

spontaneous rupture simulations that do not include the preceding parts of the earthquake cycles and far-field loading, the nucleation process is often artificial (a prescribed initial condition), and its choice affects results (Bizzarri, 2010). Prescribing higher initial shear stress or decreasing the strength within the nucleation zone has been commonly used to artificially nucleate ruptures in simulations (e.g., Harris et al., 2009).

To successfully initiate a spontaneous rupture, the nucleation zone needs to be larger than a critical size (e.g., Day, 1982; Galis et al., 2015),

$$A_1 = \frac{(3\pi)^3}{2^{11}} \frac{\tau_0 - \tau_d}{\tau_0^i - \tau_0} \frac{(\tau_s - \tau_d)^2}{(\tau_0 - \tau_d)^4} \mu^2 d_0^2, \tag{2}$$

in which the τ_s,τ_d,τ_0 represent yield strength, dynamic stress and initial stress on ambient fault, τ_0^i is the initial shear stress within the nucleation zone, and μ and d_0 are shear modulus and critical slip distance, respectively. Such relation is derived based on a uniform initial stress and strength distribution and nucleating

the rupture by increasing initial stress. Because the initial stress distribution is heterogeneous in our models, we nucleate ruptures by decreasing strength to be 0.1 MPa lower than the average initial stress within a circular nucleation zone, and therefore we modify the above equation

$$A_1 = \frac{(3\pi)^3}{2^{11}} \frac{\overline{\tau_0 - \tau_d}}{\tau_s - \tau_s^i} \frac{(\tau_s - \tau_d)^2}{(\overline{\tau_0 - \tau_d})^4} \mu^2 d_0^2 \quad (3)$$

where $\overline{\tau_0 - \tau_d}$ and $(\tau_s - \tau_s^i)$ denote average static stress drop and strength decrease within the nucleation zone, respectively. The minimum size of the nucleation zone depends on the location and the area size because of the heterogeneous stress distribution.

4.2. Dynamic Rrupture Scenario of the 2012 Nicoya Earthquake

We first derive rupture scenarios from the locking models based on a uniform strength distribution, slightly higher than the maximum initial stress (i.e., 20.5 MPa). Because we need to make meaningful comparison with the kinematic source model of the 2012 Nicoya earthquake, we force the nucleation from the hypocenter (Yue et al., 2013), which locates in relatively low stress areas in our models and thus requires an unrealistically large nucleation zone (>100 km^2) by only decreasing the strength. Since a radius of 5-km nucleation zone approximately corresponds to an Mw 6 earthquake, we therefore consider it as the upper limit in our nucleation zone sizes to minimize artificial effects on the modeled moment magnitudes of rupture scenarios. However, the rupture does not successfully propagate outside the nucleation zone by only decreasing the strength or increasing initial stress (Figure S3).

To generate a rupture with comparable size of the 2012 Nicoya earthquake, we then conduct a series of nucleation tests by ensuring a reasonable rupture speed (<0.8 *V*s) until the rupture becomes spontaneously dynamic. This is also termed time weakening (e.g., Andrews, 1985; Harris et al., 2018). Through the trial-and-error process, we eventually increased the initial stress to 15.5 MPa in a circle with a radius of 7 km and decreased the strength to 14 MPa in a 2.5-km-radius circle for the Xue locking model, both being centered at the hypocenter of the 2012 Nicoya earthquake. In such case, the rupture can propagate out of the nucleation zone with a reasonable rupture speed (~0.6 *V*s).

The rupture starts in a circular patch and first propagates downdip due to the direction of concentrated stress (Figure 4a). Then part of the rupture starts to propagate updip, forming a bilateral rupture (Figure 4b). After 12 s, the rupture propagates primarily along strike until arrest (Figures 4c–4f). The rupture is initially dominated by crack mode and then evolves into slip pulse around 15 s (Figure 5). Peak slip rates reach ~5 m/s, correlating with high-locking regions (Figure 5f). The total duration of the rupture is ~30 s with an average rupture speed of ~2.7 km/s. The rupture area spans ~75 km downdip and ~100 km along strike (Figure 4f), resulting in a total seismic moment of 2.7×10^{20} Nm and $M_W = 7.6$ with the maximum slip of 4.5 m, consistent with the kinematic source models (Protti et al., 2014; Yue et al., 2013).

We also derive rupture scenarios from the Feng locking model, following the same procedure. The rupture also starts to propagate downdip, then updip, following by along-strike expansion until arrest (Figure 6). The downdip part of the rupture evolves into slip pulse after 10 s. Peak slip rates are ~5 m/s and also correlate well with high-locking areas (Figure 7), similar to those in the Xue locking model. The rupture area covers ~80 km along strike (Figure 6f), slightly smaller than that in the Xue locking model. However, the final moment magnitude of the scenario earthquake is Mw 7.55, similar to that of the 2012 Nicoya earthquake.

In addition to the total moment and peak slip, we compare the slip distribution and moment rate function in our dynamic model with those in the kinematic models. The simulated slip distributions in both locking models (slip >1 m) correlate well with the inversions from observations, especially for the on-shore patch (Figures 8a and 8b), despite that the inverted slip extended to greater depth than those predicted from locking models. Furthermore, our modeled moment rate from the Xue model shows a single peak value of ~2.6×10^{19} Nm/s at ~15 s (Figure 8c). The slope of the moment rate function is quite sharp in the first 10 s with a relatively fast rupture speed of ~3 km/s. Both the peak value and the shape of the moment rate function are consistent with those in the kinematic models (Quintero et al., 2014; Ye et al., 2013). In contrast, the scenario from Feng locking model exhibits two peaks in the moment rate (Figure 8c), which attribute to the effects of heterogeneous initial stress distribution on rupture propagation.

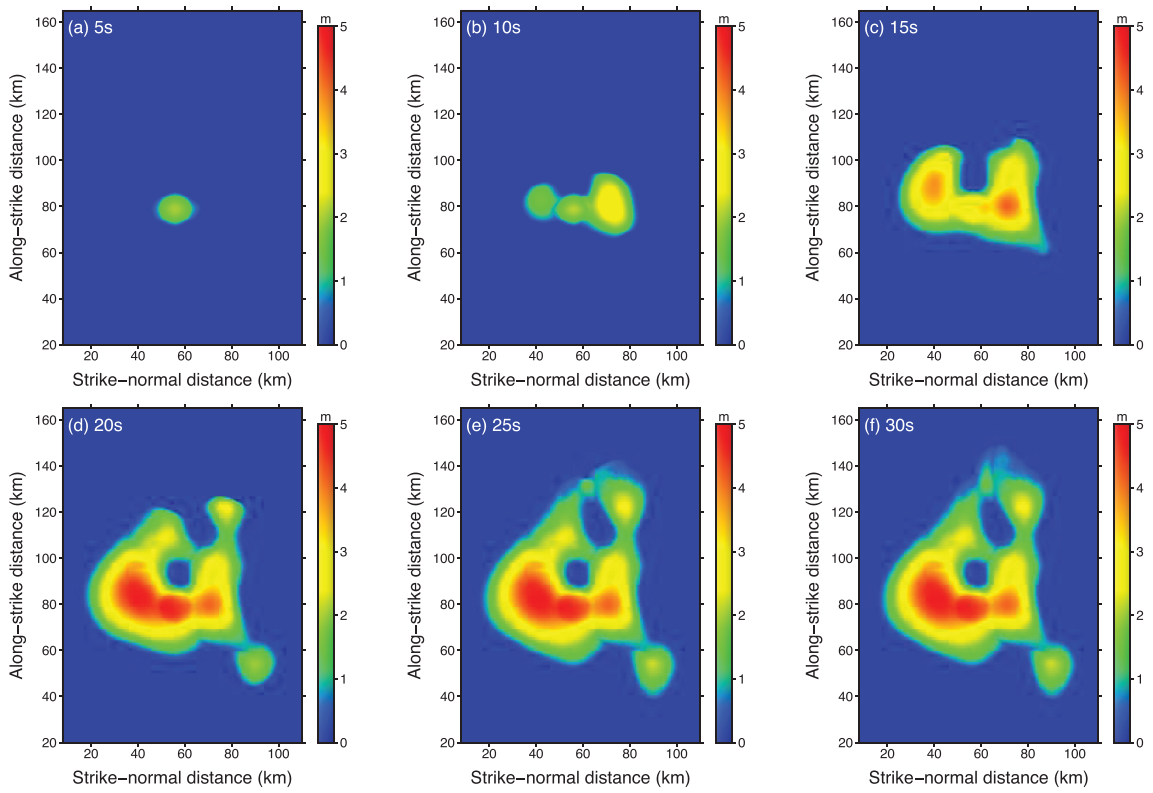

Figure 4. Snapshot in every 5 s of the slip amplitude (color) of the scenario derived from the Xue locking model.

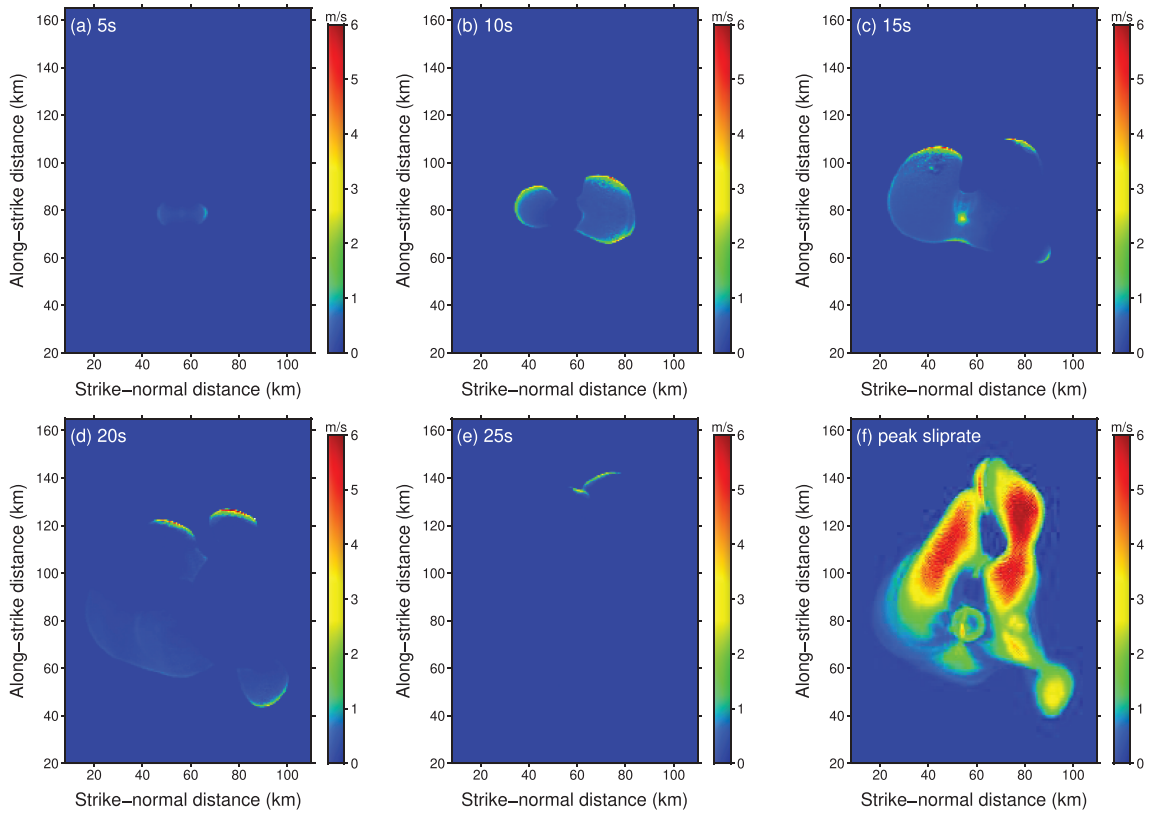

Figure 5. Snapshot in every 5 s of slip rate (color) on the fault (a–e). (f) Peak slip rate distribution on the fault.

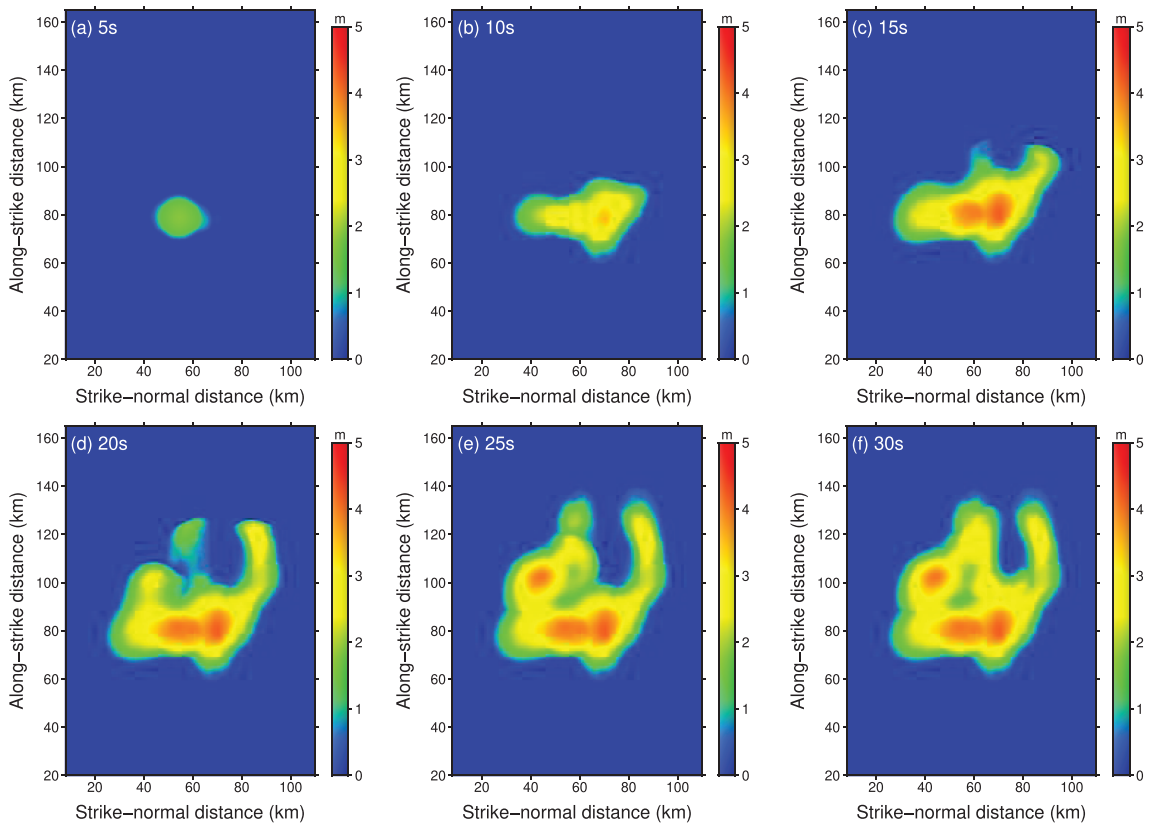

Figure 6. Same to Figure 4, except for the Feng locking model.

5. Discussion

5.1. Effects of Along-Strike Variation in Strength Distribution

Using a uniform distribution of strength and critical slip distance, we demonstrate that deriving a reasonable approximation of the coseismic slip distribution and rupture process from interseismic locking is feasible. In both scenarios, the final moment magnitudes and main slip locations are consistent with those of the 2012 Mw 7.6 Nicoya earthquake. However, there are appreciable differences between our dynamic model and the kinematic ones. Both locking models over predict slip in the northwest offshore region (Figures 8a and 8b), as it is prescribed with high interseismic locking. The simulated ruptures will break the high-stress patch unless additional heterogeneities are introduced.

Rupture propagation is not only affected by the initial stress distribution but also depends on strength heterogeneities on the fault (e.g., Weng et al., 2015; Yang et al., 2012). In the above rupture scenarios, we employ a uniform strength distribution. However, seismic receiver function images have been used to infer that fault strength is higher in the northwestern part of the East Pacific Rise-Cocos-Nazca suture than in the southeast (Audet & Schwartz, 2013). But the along-strike changes in fault strength have not been quantified. We conduct a test by prescribing a higher strength (i.e., 22.5 MPa) in the northwest and a lower value (i.e., 18.5 MPa) in the northeast (rupture scenario 2 in Table 1), and find that such along-strike variation in strength slightly improved the fit between the dynamic and kinematic models in final slip distribution (Figure 9a). However, the rupture duration is shortened because the rupture did not propagate further northward (Figure 9b). Moment magnitude is slightly reduced but is still consistent with observation.

To better quantify potential rupture scenarios from interseismic locking models, well-determined strength distributions on the megathrust will be helpful. Due to the limitation in direct measurement of stress state and pore fluid pressure on seismogenic faults, strength distributions are poorly known and usually estimated from other observations or calculations. During major earthquakes, the “strength drop” (described as the

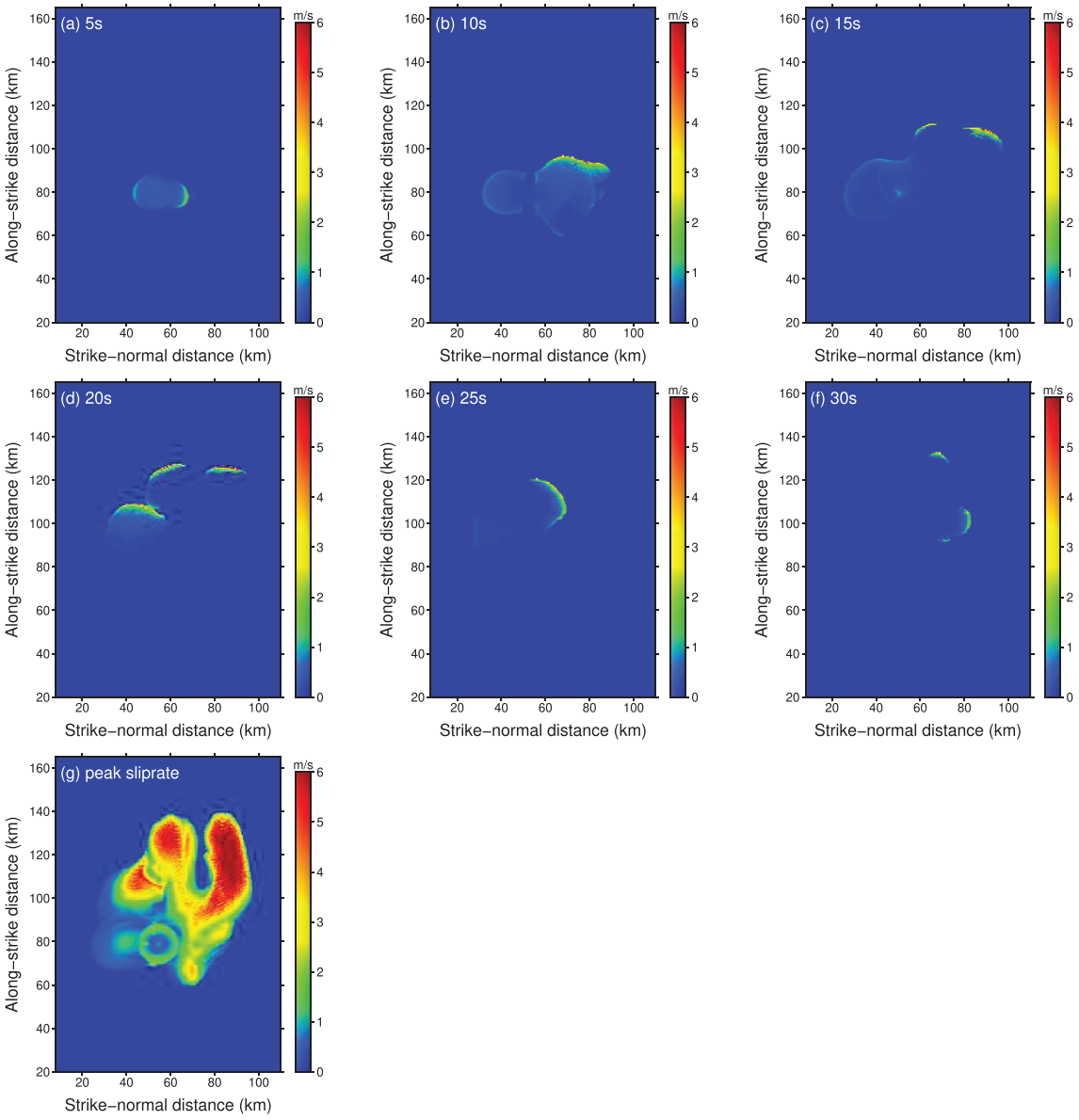

Figure 7. Same to Figure 5, except for the Feng locking model.

reduction in frictional resistance from static to dynamic friction) may be used to infer a ruptured fault's strength distribution, when assuming a constant dynamic stress (Weng & Yang, 2018). As such, we can conduct dynamic rupture simulations to evaluate the strength drop during the 2012 Nicoya earthquake using constraints from near-field observations. From these, we can better quantify details in rupture scenarios from interseismic locking models. Because this process is computationally expensive and is beyond the scope of the current work, we may explore it in future studies.

5.2. Synthetic Ground Velocities

We compute synthetic ground velocities in our modeled scenarios at the six high-rate GPS locations (Figure 1), at which the 2012 Nicoya earthquake was well recorded. We obtain three-component processed ground motion data of the high-rate GPS measurements from Yin and Wdowinski (2014). We transform the time series of displacement into velocity waveforms and apply a bandpass filter of 0.05–0.25 Hz. Then we rotate the horizontal components into along-strike and strike-normal directions. The synthetic ground velocities are filtered to the same band as Yue et al. (2013) and appear largely consistent with the observations in

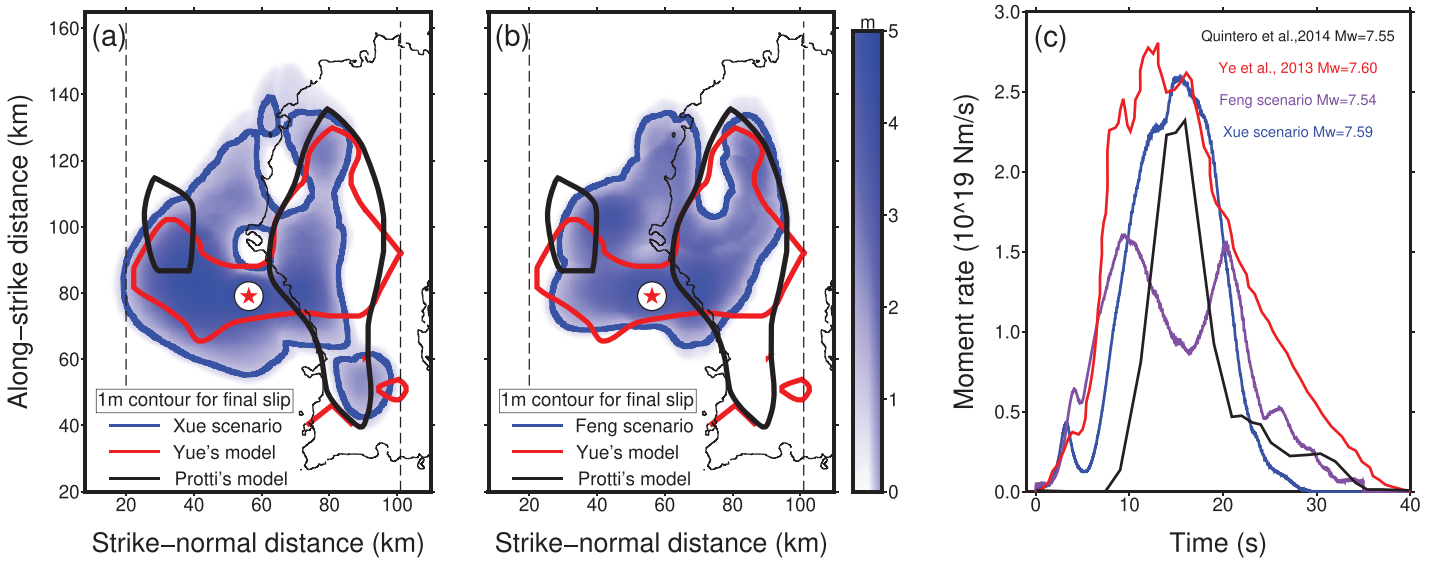

Figure 8. (a) Coseismic slip distribution from numerical rupture scenario derived from the Xue locking model (blue), and kinematic source models (red: Yue et al., 2013; black: Protti et al., 2014), (b) final slip distribution from the Feng locking model, (c) moment rate functions from the numerical rupture scenarios (blue and purple), and two other kinematic source models (Quintero et al., 2014; Ye et al., 2013).

both waveform shapes and amplitudes (Figure 10), especially on the vertical components. At certain stations, for example, SAJU and HATI, the modeled amplitudes of ground velocities are larger than observations (Figure 10) because of the over-predicted slip offshore near the two stations (Figure 8a).

Synthetic waveforms from the Feng locking model agree with the observations to some extents, for example, the first pulse in the data (Figure 11). However, the discrepancies appear larger than those from the Xue model. For instance, the second pulses in the synthetics appear at a few stations (PUJE, CABA, and EPZA) but are not visible in the data (Figure 11). Such discrepancies originate from the detailed rupture processes, despite nearly identical moment magnitudes obtained from both locking models. The moment rate in the Feng locking model exhibits two peaks (Figure 8c), implying two subevents during the 2012 Nicoya earthquake. However, no kinematic solutions have claimed subevents of the Nicoya quake, and both kinematic models show a single peak in the moment rate function (Quintero et al., 2014; Ye et al., 2013). Therefore, we conclude that the coseismic scenarios derived from the Xue locking model appear to better

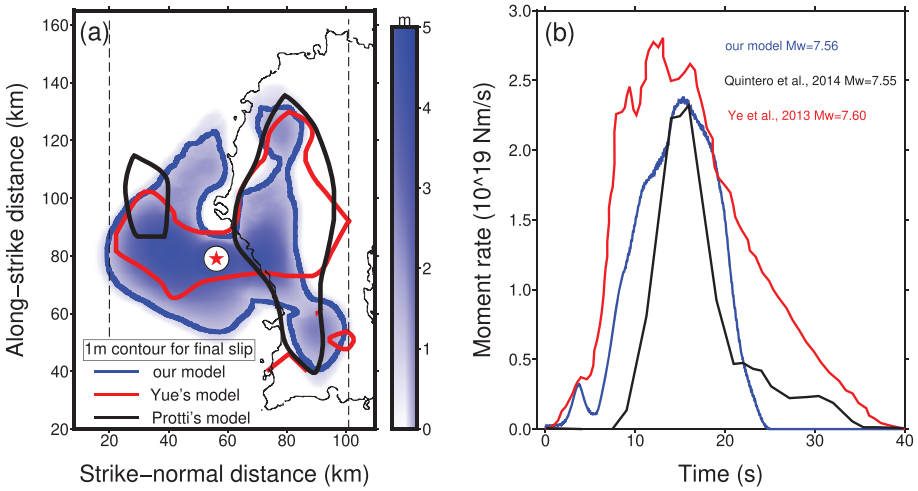

Figure 9. Same to Figure 8, except for along-strike variation of fault strength.

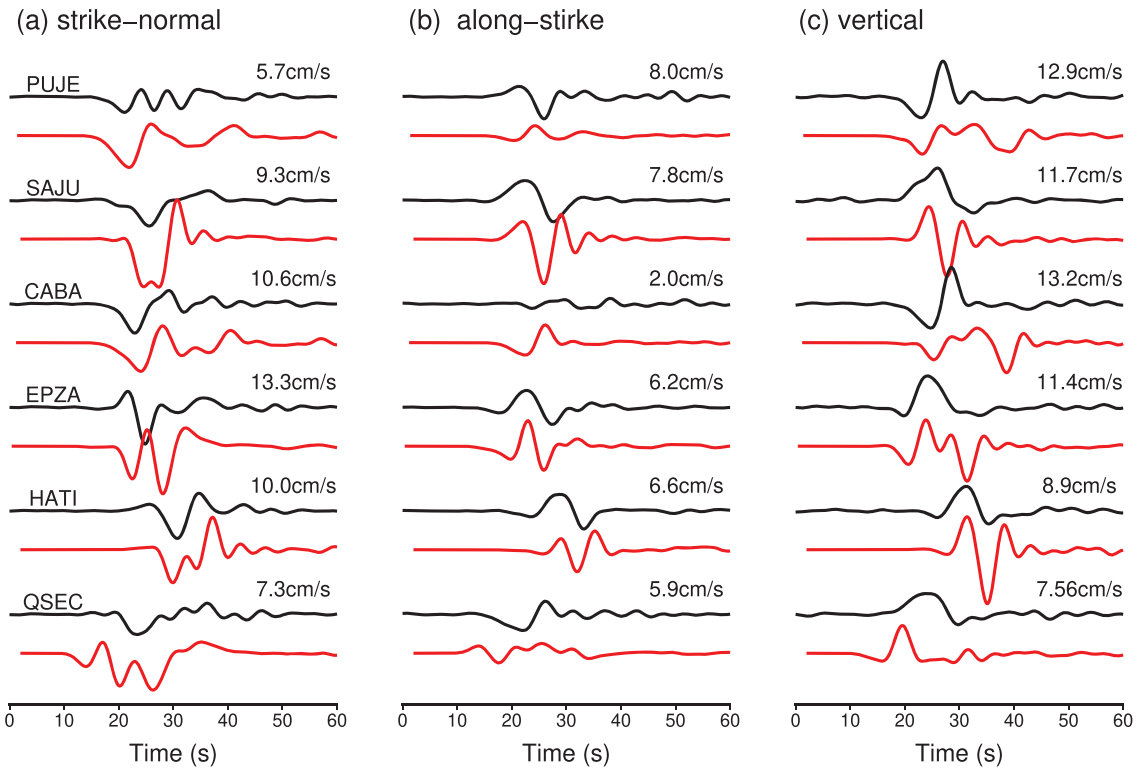

Figure 10. Comparison between synthetic ground velocities (red) with near-field high-rate global positioning system recordings (black). Station names and peak ground velocities are marked on each data trace.

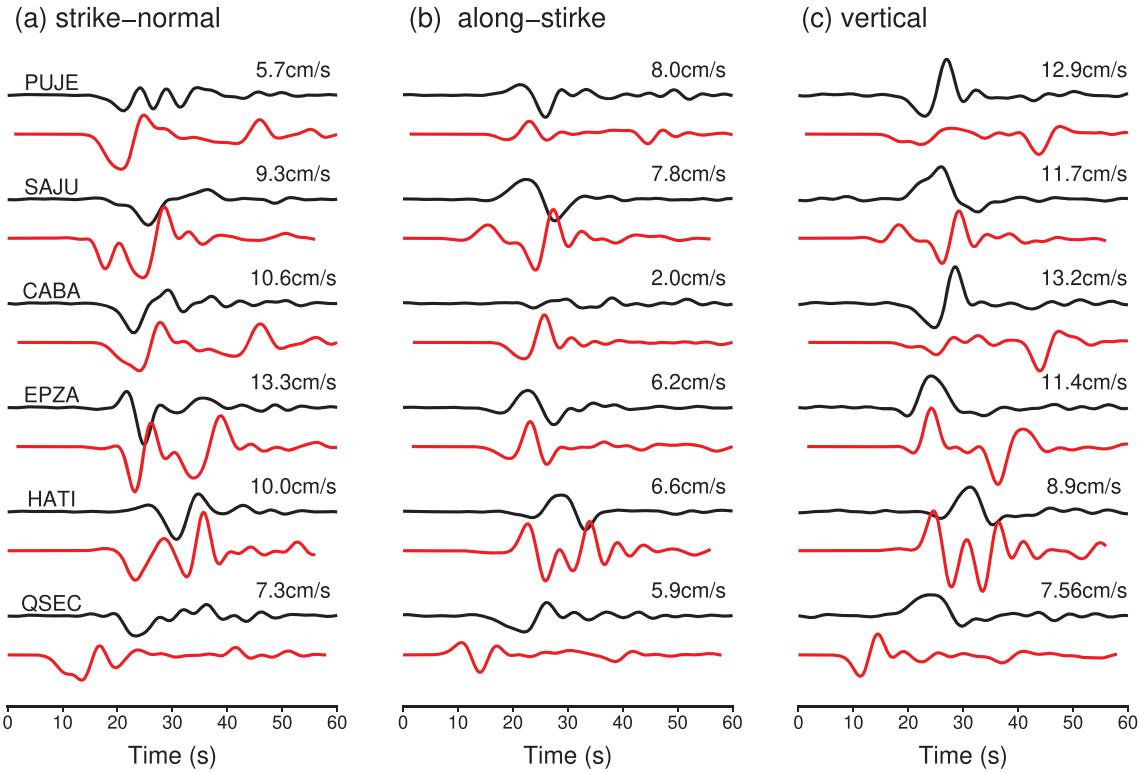

Figure 11. Same to Figure 10, except for synthetics computed from the Feng locking model.

fit the kinematic model of Yue et al. (2013) than did the scenarios from the Feng locking model. While the Feng locking model used trench-normal and vertical GPS along a curviplanar megathrust, the Xue locking model also incorporated trench-parallel GPS and interferometric synthetic aperture radar data along the same geometry that may have improved some resolution of features.

5.3. Earthquake Initiation from Low-Locking Region

The hypocenter of the 2012 Nicoya earthquake locates in a relatively low-locking region (Figure 1). Similarly, a few megathrust earthquakes were suggested to initiate from moderate to low locking areas offshore, such as the 2011 Mw 9.0 Tohoku-Oki earthquake (e.g., Simons et al., 2011) and the 2007 Mw 8.4 Mentawai earthquake (Konca et al., 2008), although the locking distribution offshore was generally not well constrained without seafloor geodetic measurements.

Since we estimated initial stress from locking, the stress level corresponds to the spatial gradient of the locking distribution that is directly controlled by the model resolution. In the Nicoya region, the spatial variation of locking degree is rather smooth, which may reflect the limited resolution (>20 km) of the locking models. We are not able to resolve more spatially heterogeneous stress distribution unless locking models with much higher resolution become available. Therefore, we cannot rule out that the Nicoya earthquake initiated from a small high-stress spot, which was however not captured by locking models.

5.4. Other Challenges in Deriving Coseismic Slip from Locking Distributions

In addition to the spatial resolution in locking models, patterns of fault locking do not necessarily correspond to earthquake rupture extent. One of the reasons is the stress shadowing effect, in which a patch reaching the failure state cannot move because of strong locking of neighboring patches (Wang, 2007). The effects may be quite strong near trench due to the downdip locked megathrust (Almeida et al., 2018). In a 2-D boundary element model, a shallow velocity-strengthening patch can only creep at most 30% of the plate convergence rate. As such, the locking model derived from geodetic measurements may underestimate the degree of locking on shallow megathrust and thus earthquake and tsunami hazard (Almeida et al., 2018). Such stress shadowing effect, together with uncertainties of locking models near trench, needs to be quantitatively evaluated for tsunamic hazard assessment by spontaneous rupture simulations, considering a number of ad hoc models.

Moreover, stress history evolves on seismogenic faults, especially in subduction zones where frequent megathrust earthquakes occurred, posing challenges to accurately estimate the slip deficit from locking models. For example, a locked segment remains unbroken between the 2010 Mw 8.8 Maule and 2015 Mw 8.3 Illapel, Chile earthquakes that ruptured a portion of the highly locked patch, respectively (Moreno et al., 2010; Yin et al., 2016). It is unclear whether the failure of breaking the locked segment during the past two megathrust ruptures was due to low stress or geometric changes on the megathrust (Bletery et al., 2016; Qiu et al., 2016; Yang et al., 2013; Yu et al., 2018). Detailed rupture histories in a locked segment are crucial for estimating future rupture potential and deriving detailed scenarios. Fortunately, the M7.5+ megathrust earthquakes recur in Nicoya with an approximate 50-year period, the last taking 62 years. In the last interseismic period, there were few interplate earthquakes of significant magnitude, providing an ideal environment to derive rupture scenarios from slip deficit calculations.

Additional factors such as dynamic weakening processes may modulate rupture propagation (e.g., Noda & Lapusta, 2013; Rice, 2006). Different dynamic weakening mechanisms have been explored and tested in laboratory experiments (e.g., Di Toro et al., 2011; Wibberley & Shimamoto, 2005; Yao et al., 2018). Regardless of rock composition and experimental conditions in the laboratory, strong weakening behaviors have been observed under seismic slip rates, termed velocity weakening. Some mechanisms (e.g., thermal pressurization) are used to explain field observations of large slip in the velocity-strengthening region (Noda & Lapusta, 2013). However, these effects are not considered in this study, as their relevant parameters on the megathrust are poorly known and we do not know whether such mechanisms occurred during the Nicoya earthquake. Furthermore, numerical results based on velocity-weakening law do not qualitatively differ with those using slip-weakening law (Gabriel et al., 2012; Luo & Duan, 2018; Murphy et al., 2018). As such, our results derived from the linear slip-weakening law should be, at least qualitatively, no different from those incorporating more complex effects, if relevant frictional parameters on the megathrust can be well constrained from independent observations.

6. Conclusions

Here we demonstrate that deriving rupture scenarios from interseismic locking models is feasible in the Nicoya Peninsula, Costa Rica. Our dynamic rupture simulations show consistent final slip distribution, moment magnitude, and moment rate function with those of the 2012 Mw 7.6 Nicoya earthquake from one of the locking models (Xue et al., 2015). Our synthetic ground velocities also agree with near-field high-rate GPS observations during the 2012 earthquake. We also find that the rupture scenarios are dependent on the choice of input locking models, highlighting the necessity to quantitatively investigate detailed rupture scenarios from interseismic locking models. This study provides a framework to quantitatively evaluate potential earthquake sizes from interseismic locking models, which can be used for other subduction zones that have reasonably well-constrained locking distribution. Such an approach can be further improved by constraining a priori frictional parameters on seismogenic faults using near-field observations and/or incorporating dynamic weakening mechanisms that impact earthquake rupture propagation.

Data Availability Statement

All data and results in this study are generated from numerical simulations. Digital files can be accessible from https://drive.google.com/open?id=190O8OaV9h2uv4kFXVKFPSWQpgGGIVsoR. High-rate GPS data are from https://www.unavco.org/data/gps-gnss/gps-gnss.html.

Acknowledgments
The authors thank support from Hong Kong Research Grant Council grants (24601515, 14313816, and 14306418), China Earthquake Science Experiment Project, CEA (grant no. 2017CESE0103), CUHK Direct Grant from Faculty of Science, Open Fund of the State Key Lab of Earthquake Dynamics (grant no. LED2017B07), Institute of Geology, CEA, and US National Science Foundation grant to AVN (1447104). We also benefit from constructive comments from the associate editor Alice-Agnes Gabriel and three anonymous reviewers.

References

Aagaard, B. T., Knepley, M. G., & Williams, C. A. (2013). A domain decomposition approach to implementing fault slip in finite-element models of quasi-static and dynamic crustal deformation. *Journal of Geophysical Research: Solid Earth*, *118*, 3059–3079. https://doi.org/10.1002/jgrb.50217

Almeida, R., Lindsey, E. O., Bradley, K., Hubbard, J., Mallick, R., & Hill, E. M. (2018). Can the updip limit of frictional locking on mega-thrusts be detected geodetically? Quantifying the effect of stress shadows on near-trench coupling. *Geophysical Research Letters*, *45*, 4754–4763. https://doi.org/10.1029/2018GL077785

Ampuero, J. P., Vilotte, J. P., & Sanchez-Sesma, F. (2002). Nucleation of rupture under slip dependent friction law: Simple models of fault zone. *Journal of Geophysical Research*, *107*(B12), 2324. https://doi.org/10.1029/2001JB000452

Andrews, D. (1976). Rupture propagation with finite stress in antiplane strain. *Journal of Geophysical Research*, *81*(20), 3575–3582.

Andrews, D. (1985). Dynamic plane-strain shear rupture with a slip-weakening friction law calculated by a boundary integral method. *Bulletin of the Seismological Society of America*, *75*(1), 1–21.

Audet, P., & Schwartz, S. Y. (2013). Hydrologic control of forearc strength and seismicity in the Costa Rican subduction zone. *Nature Geoscience*, *6*(10), 852–855.

Avants, M., Schwartz, S., Newman, A., & Deshon, H. (2001). Large underthrusting earthquakes beneath the Nicoya Peninsule, *Eos Trans. AGU, 82*(46), Fall meet. Suppl., Abstract T52E-07.

Barckhausen, U.,Ranero, C. R., Huene, R.,Cande, S. C., & Roeser, H. A. (2001). Revised tectonic boundaries in the Cocos Plate off Costa Rica: Implications for the segmentation of the convergent margin and for plate tectonic models. *Journal of Geophysical Research*, *106*(B9), 19,207– 19,220. https://doi.org/10.1029/2001JB000238

Bizzarri, A. (2010). How to promote earthquake ruptures: Different nucleation strategies in a dynamic model with slip-weakening friction. *Bulletin of the Seismological Society of America*, *100*, 923–940.

Bletery, Q., Thomas, A. M., Rempel, A. W., Karlstrom, L., Sladen, A., & De Barros, L. (2016). Mega-earthquakes rupture flat megathrusts. *Science*, *354*(6315), 1027–1031. https://doi.org/10.1126/science.aag0482

Bruhat, L., & Segall, P. (2017). Deformation rates in northern Cascadia consistent with slow updip propagation of deep interseismic creep. *Geophysical Journal International*, *211*, 427–449. https://doi.org/10.1093/gji/ggx317

Burgette, R. J., Weldon, R. J., & Schmidt, D. A. (2009). Interseismic uplift rates for western Oregon and along-strike variation in locking on the Cascadia subduction zone. *Journal of Geophysical Research*, *114*, B01408. https://doi.org/10.1029/2008JB005679

Day, S. M. (1982). Three-dimensional finite difference simulation of fault dynamics: Rectangular faults with fixed rupture velocity. *Bulletin of the Seismological Society of America*, *72*, 705–727.

Day, S. M., Dalguer, L. A., Lapusta, N., & Liu, Y. (2005). Comparison of finite difference and bounday in tegral solutions to three-dimensional spontaneous rupture. *Journal of Geophysical Research*, *110*, B12307. https://doi.org/10.1029/2005JB003813

DeMets, C., Gordon, R. G., & Argus, D. F. (2010). Geologically current plate motions. *Geophysical Journal International*, *181*, 1–80. https://doi.org/10.1111/j.1365-246X.2009.04491.x

DeShon, H. R., Schwartz, S. Y., Newman, A. V., Gonzalez, V., Protti, M., Dorman, L. R. M., et al. (2006). Seismogenic zone structure beneath the Nicoya Peninsula, Costa Rica, from three-dimensional local earthquake P- and S-wave tomography. *Geophysical Journal International*, *164*(1), 109–124. https://doi.org/10.1111/j.1365-246X.2005.02809.x

Di Toro, G., Han, R., Hirose, T., De Paola, N., Nielsen, S., Mizoguchi, K., et al. (2011). Fault lubrication during earthquakes. *Nature*, *471* (7339), 494–498. https://doi.org/10.1038/nature09838

Dixon, T. H., Jiang, Y., Malservisi, R., McCaffrey, R., Voss, N., Protti, M., & Gonzalez, V. (2014). Earthquake and tsunami forecasts: Relation of slow slip events to subsequent earthquake rupture. *Proceedings of the National Academy of Sciences of the United States of America*, *111*(48), 17,039–17,044. https://doi.org/10.1073/pnas.1412299111

Ellsworth, W. L., & Bulut, F. (2018). Nucleation of the 1999 Izmit earthquake by a triggered cascade of foreshocks. *Nature Geoscience*, *11*, 531–535.

Feng, L., Newman, A. V., Protti, M., Gonzalez, V., Jiang, Y., & Dixon, T. H. (2012). Active deformation near the Nicoya Peninsula, northwestern Costa Rica, between 1996 and 2010: Interseismic megathrust coupling. *Journal of Geophysical Research*, *117*, B06407. https://doi.org/10.1029/2012JB009230

Gabriel, A. A., Ampuero, J. P., Dalguer, L. A., & Mai, P. M. (2012). The transition of dynamic rupture styles in elastic media under velocity-weakening friction. *Journal of Geophysical Research*, *117*, B09311. https://doi.org/10.1029/2012JB009468

Galis, M., Pelties, C., Kristek, J., Moczo, P., Ampuero, J.-P., & Mai, P. M. (2015). On the initiation of sustained slip-weakening ruptures by localized stresses. *Geophysical Journal International*, *200*(2), 890–909.

Guatteri, M., & Spudich, P. (2000). What can strong-motion data tell us about slip-weakening fault-friction laws? *Bulletin of the Seismological Society of America*, *90*(1), 98–116.

Harris, R. A. (2004). Numerical simulations of larger earthquakes: Dynamic rupture propagation on heterogeneous faults. In A. Donnellan, P. Mora, M. Matsu'ura, & X. Yin (Eds.), *Computational Earthquake Science Part II* (pp. 2171–2181). Basel: PAGEOPH Topical Volumes. Birkhäuser. https://doi.org/10.1007/978-3-0348-7875-3_5

Harris, R. A., Barall, M., Aagaard, B., Ma, S., Roten, D., Olsen, K., et al. (2018). A suite of excercises for verifying dynamic earthquake rupture codes. *Seismological Research Letters*, *89*(3), 1146–1162. https://doi.org/10.1785/0220170222

Harris, R. A., Barall, M., Archuleta, R., Dunham, E., Aagaard, B., Ampuero, J. P., et al. (2009). The SCEC/USGS dynamic earthquake rupture code verification exercise. *Seismological Research Letters*, *80*(1), 119–126. https://doi.org/10.1785/gssrl.80.1.119

Harris, R. N., Spinelli, G., Ranero, C. R., Grevemeyer, I., Villinger, H., & Barckhausen, U. (2010). Thermal regime of the Costa Rican convergent margin: 2. Thermal models of the shallow Middle America subduction zone offshore Costa Rica. *Geochemistry, Geophysics, Geosystems*, *11*, Q12S29. https://doi.org/10.1029/2010GC003273

Hok, S., Fukuyama, E., & Hashimoto, C. (2011). Dynamic rupture scenarios of anticipated Nankai-Tonankai earthquakes, southwest Japan. *Journal of Geophysical Research*, *116*, B12319. https://doi.org/10.1029/2011JB008492

Ida, Y. (1972). Cohesive force across the tip of a longitudinal-shear crack and Griffith's specific surface energy. *Journal of Geophysical Research*, *77*(20), 3796–3805.

Kaneko, Y., Avouac, J.-P., & Lapusta, N. (2010). Towards inferring earthquake patterns from geodetic observations of interseismic coupling. *Nature Geoscience*, *3*, 363–369.

Konca, A. O., Avouac, J. P., Sladen, A., Meltzner, A. J., Sieh, K., Fang, P., et al. (2008). Partial rupture of a locked patch of the Sumatra megathrust during the 2007 earthquake sequence. *Nature*, *456*(7222), 631–635. https://doi.org/10.1038/nature07572

Liu, C., Zheng, Y., Xiong, X., Wang, R., López, A., & Li, J. (2015). Rupture processes of the 2012 September 5 Mw 7.6 Nicoya, Costa Rica earthquake constrained by improved geodetic and seismological observations. *Geophysical Journal International*, *203*(1), 175–183. https://doi.org/10.1093/gji/ggv295

Loveless, J. P., & Meade, B. J. (2011). Spatial correlation of interseismic coupling and coseismic rupture extent of the 2011 Mw = 9.0 Tohoku-oki earthquake. *Geophysical Research Letters*, *38*, L17306. https://doi.org/10.1029/2011GL048561

Lozos, J. C., Harris, R. A., Murray, J. R., & Lienkaemper, J. J. (2015). Dynamic rupture models of earthquakes on the Bartlett Springs Fault, Northern California. *Geophysical Research Letters*, *42*, 4343–4349. https://doi.org/10.1002/2015GL063802

Luo, B., & Duan, B. (2018). Dynamics of nonplanar thrust faults governed by various friction laws. *Journal of Geophysical Research: Solid Earth*, *123*, 5147–5168. https://doi.org/10.1029/2017JB015320

Madariaga, R. (1976). Dynamics of an expanding circular fault. *Bulletin of the Seismological Society of America*, *66*(3), 639–666.

McCaffrey, R., Qamar, A. I., King, R. W., Wells, R., Khazaradze, G., Williams, C. A., et al. (2007). Fault locking, block rotation and crustal deformation in the Pacific Northwest. *Geophysical Journal International*, *169*(3), 1315–1340. https://doi.org/10.1111/j.1365-246X.2007.03371.x

Meade, B. J. (2007). Algorithms for the calculation of exact displacements, strains, and stresses for triangular dislocation elements in a uniform elastic half space. *Computational Geosciences*, *33*, 1064–1075.

Metois, M., Socquet, A., Vigny, C., Carrizo, D., Peyrat, S., Delorme, A., et al. (2013). Revisiting the North Chile seismic gap segmentation using GPS-derived interseismic coupling. *Geophysical Journal International*, *194*, 1283–1294. https://doi.org/10.1093/gji/ggt183

Moreno, M., Rosenau, M., & Oncken, O. (2010). 2010 Maule earthquake slip correlates with pre-seismic locking of Andean subduction zone. *Nature*, *467*(7312), 198–202.

Murphy, S., Di Toro, G., Romano, F., Scala, A., Lorito, S., Spagnuolo, E., et al. (2018). Tsunamigenic earthquake simulations using experimentally derived friction laws. *Earth and Planetary Science Letters*, *486*, 155–165.

Noda, H., & Lapusta, N. (2013). Stable creeping fault segments can become destructive as a result of dynamic weakening. *Nature*, *493*, 518–521.

Olsen, K., Madariaga, R., & Archuleta, R. (1997). Three-dimensional dynamic simulation of the 1992 Landers earthquake. *Science*, *278*(5339), 834–838.

Palmer, A. C., & Rice, J. R. (1973). The growth of slip surfaces in the progressive failure of over-consolidated clay. *Proceeding of the Royal Society of London*, *332*, 527–548.

Perfettini, H., Avouac, J.-P., Tavera, H., Kositsky, A., Nocquet, J.-M., Bondoux, F., et al. (2010). Seismic and aseismic slip on the Central Peru megathrust. *Nature*, *456*, 78–81. https://doi.org/10.1038/nature09062

Protti, M., González, V., Newman, A. V., Dixon, T. H., Schwartz, S. Y., Marshall, J. S., et al. (2014). Nicoya earthquake rupture anticipated by geodetic measurement of the locked plate interface. *Nature Geoscience*, *7*(2), 117–121. https://doi.org/10.1038/ngeo2038

Protti, M., Güendel, F., & Malavassi, E. (2001). *Evaluación del potencialsísmico de laPeninsula de Nicoya, Heredia*, (p. 144). Editorial Fundación UNA: Costa Rica.

Qiu, Q., Hill, E. M., Barbot, S., Hubbard, J., Feng, W., Lindsey, E. O., et al. (2016). The mechanism of partial rupture of a locked megathrust: The role of fault morphology. *Geology*, *44*(10), 875–878.

Quintero, R., Zahradník, J., & Sokos, E. (2014). Near-regional CMT and multiple-point source solution of the September 5, 2012, Nicoya, Costa Rica Mw 7.6 (GCMT) earthquake. *Journal of South American Earth Sciences*, *55*, 155–165.

Rice, J. R. (2006). Heating and weakening of faults during earthquake slip. *Journal of Geophysical Research*, *111*, B05311. https://doi.org/10.1029/2005JB004006

Saffer, D. M., & Tobin, H. J. (2011). Hydrogeology and mechanics of subduction forearcs: Fluid flow and pore pressure. *Annual Review of Earth and Planetary Sciences*, *39*(1), 157–186.

Satake, K., & Atwater, B. F. (2007). Long-term perspectives on giant earthquakes and tsunamis at subduction zones. *Annual Review of Earth and Planetary Sciences*, *35*, 349–374.

Simons, M., Minson, S. E., Sladen, A., Ortega, F., Jiang, J., Owen, S. E., et al. (2011). The 2011 magnitude 9.0 Tohoku-Oki earthquake: Mosaicking the megathrust from seconds to centuries. *Science*, *332*(6036), 1421–1425. https://doi.org/10.1126/science.1206731

Tape, C., Holtkamp, S., Silwal, V., Hawthorne, J., Kaneko, Y., Ampuero, J. P., et al. (2018). Earthquake nucleation and fault slip complexity in the lower crust of central Alaska. *Nature Geoscience*, *11*(7), 536–541. https://doi.org/10.1038/s41561-018-0144-2

Tinti, E., Spudich, P., & Cocco, M. (2005). Earthquake fracture energy inferred from kinematic rupture models on extended faults. *Journal of Geophysical Research*, *110*, B12303. https://doi.org/10.1029/2005JB003644

Wang, K. (2007). Elastic and viscoelastic models of subduction earthquake cycles. In T. H. Dixon, & J. C. Moore (Eds.), *The seismogenic zone of subduction thrust faults*, (pp. 540–575). New York: Columbia Univ. Press.

Weng, H., Huang, J., & Yang, H. (2015). Barrier-induced supershear ruptures on a slip-weakening fault.*Geophysical Research Letters*, *42*, 4824–4832. https://doi.org/10.1002/2015GL064281

Weng, H., & Yang, H. (2018). Constraining frictional properties on fault by dynamic rupture simulations and near-field observations. *Journal of Geophysical Research: Solid Earth*, *123*, 6658–6670. https://doi.org/10.1029/2017JB015414

Wibberley, C. A., & Shimamoto, T. (2005). Earthquake slip weakening and asperities explained by thermal pressurization. *Nature*, *436*(7051), 689–692.

Xue, L., Schwartz, S., Liu, Z., & Feng, L. (2015). Interseismic megathrust coupling beneath Nicoya Peninsula, Costa Rica, from the joint inversion of InSAR and GPS data. *Journal of Geophysical Research: Solid Earth*, *120*, 3707–3722. https://doi.org/10.1002/2014JB011844

Yang, H., Liu, Y., & Lin, J. (2012). Effects of subducted seamount on megathrust earthquake nucleation and rupture propagation. *Geophysical Research Letters*, *39*, L24302. https://doi.org/10.1029/2012GL053892

Yang, H., Liu, Y., & Lin, J. (2013). Geometrical effects of a subduction seamount on stopping megathrust rupture. *Geophysical Research Letters*, *40*, 2011–2016. https://doi.org/10.1002/grl.50509

Yang, H., Liu, Y. & McGuire, J. (2012). Modeling rupture segmentations on the Cascadia megathrust, *AGU Fall Meeting,* S21B-2503

Yang, H., Yao, S., He, B., & Newman, A. (2019). Earthquake rupture dependence on hypocentral location along the Nicoya Peninsula subduction megathrust. *Earth and Planetary Science Letters*, *520*, 10–17. https://doi.org/10.1016/j.epsl.2019.05.030

Yao, L., Ma, S., Chen, J., Shimamoto, T., & He, H. (2018). Flash heating and local fluid pressurization lead to rapid weakening in water-saturated fault gouges. *Journal of Geophysical Research: Solid Earth*, *123*, 9084–9100. https://doi.org/10.1029/2018JB016132

Yao, S., & Yang, H. (2018). Determination of coseismic frictional properties on the megathrust during the 2012 M7.6 Nicoya earthquake, *AGU Fall Meeting*, T41H-0407

Ye, L., Lay, T., & Kanamori, H. (2013). Large earthquake rupture process variations on the Middle America megathrust. *Earth and Planetary Science Letters*, *381*, 147–155.

Yin, H., & Wdowinski, S. (2014). Improved detection of earthquake-induced ground motion with spatial filter: Case study of the 2012 $M = 7.6$ Costa Rica earthquake. *GPS Solutions*, *18*(4), 563–570.

Yin, J., Yang, H., Yao, H., & Weng, H. (2016). Coseismic radiation and stress drop during the 2015 Mw 8.3 Illapel, Chile megathrust earthquake. *Geophysical Research Letters*, *43*, 1520–1528. https://doi.org/10.1002/2015GL067381

Yin, J., Yao, H., Yang, H., Liu, J., Qin, W., & Zhang, H. (2017). Frequency-dependent rupture process, stress change, and Seismogenic mechanism of the 25 April 2015 Nepal Gorkha Mw 7.8 earthquake. *Science China Earth Sciences*, *60*(4), 796–808.

Yu, H., Liu, Y., Yang, H., & Ning, J. (2018). Modeling earthquake sequences along the Manila subduction zone: Effects of three-dimensional fault geometry. *Tectonophysics*, *733*, 73–84. https://doi.org/10.1016/j.tecto.2018.01.025

Yue, H., Lay, T., Schwartz, S. Y., Rivera, L., Protti, M., Dixon, T. H., et al. (2013). The 5 September 2012 Nicoya, Costa Rica Mw 7.6 earthquake rupture process from joint inversion of high-rate GPS, strong-motion, and teleseismic P wave data and its relationship to adjacent plate boundary interface properties. *Journal of Geophysical Research: Solid Earth*, *118*, 5453–5466. https://doi.org/10.1002/jgrb.50379